Supporting Information

NaCl-templated synthesis of hierarchical porous carbon with extremely large specific surface area and improved graphitization degree for high energy density lithium ion capacitors

Ruiying Shi,[a, b] Cuiping Han,[c, *] Xianying Qin,[a] Xiaofu Xu,[a, b] Lei Xu,[a, b] Hongfei Li,[a] Junqin Li,[c] Ching-Ping Wong,[d, e] Baohua Li[a,*]

[a] *Engineering Laboratory for Next Generation Power and Energy Storage Batteries, Graduate School at Shenzhen, Tsinghua University, Shenzhen 518055, China*

[b] *College of Materials Science and Engineering, Shenzhen University and Shenzhen Key Laboratory of Special Functional Materials, Shenzhen 518060, China*

[c] *School of Materials Science and Engineering, Tsinghua University, Beijing, 100084, China*

[d] *School of Materials Science and Engineering, Georgia Institute of Technology, Atlanta, Georgia 30332, United State*

[e] *Department of Electronic Engineering, The Chinese University of Hong Kong, Shatin, New Territories, Hong Kong SAR, China*

*Corresponding author: Tel.: +86 755 2603 6419, Fax: +86 755 2603 6419.

E-mail address: hancuiping06@szu.edu.cn (C. Han);
libh@mail.sz.tsinghua.edu.cn (B. Li)

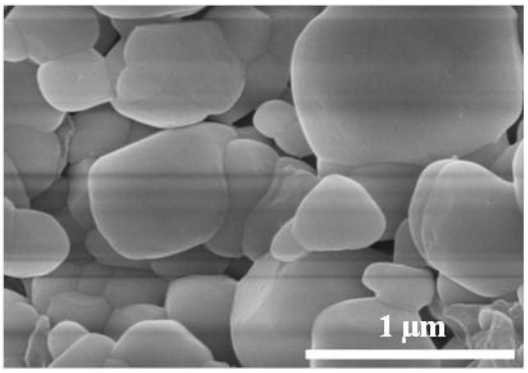

Figure S1. SEM image of protein xerogel.

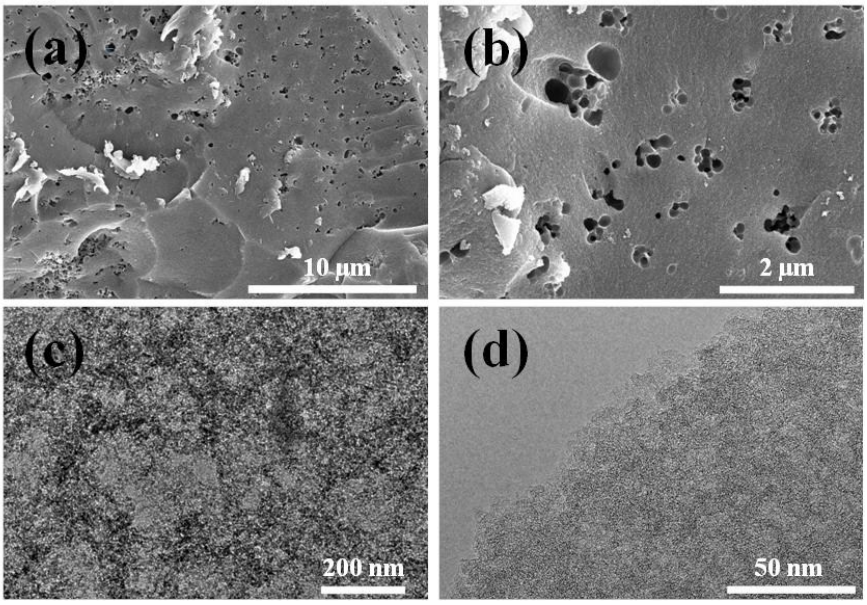

Figure S2. Morphological and structural characterization of a-EW cathode. (a~b) SEM image of a-EW, (c~d) TEM images of a-EW.

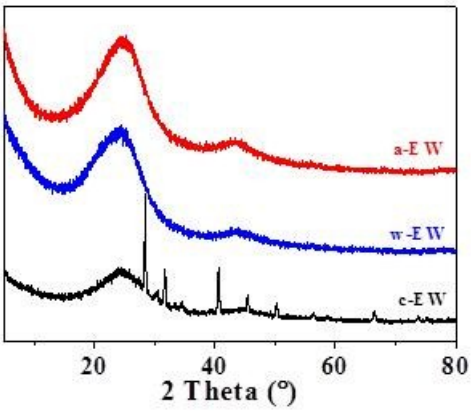

Figure S3. XRD pattern of c-EW, w-EW and a-EW.

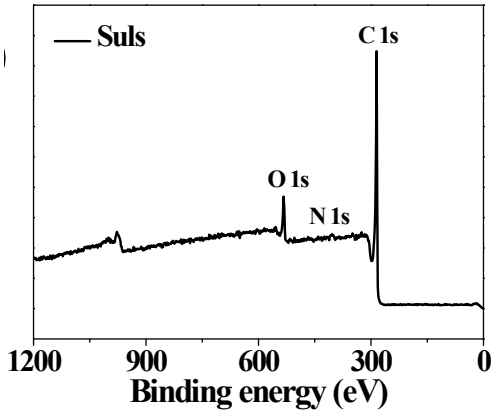

Figure S4. Survey XPS spectra of a-EW-NaCl.

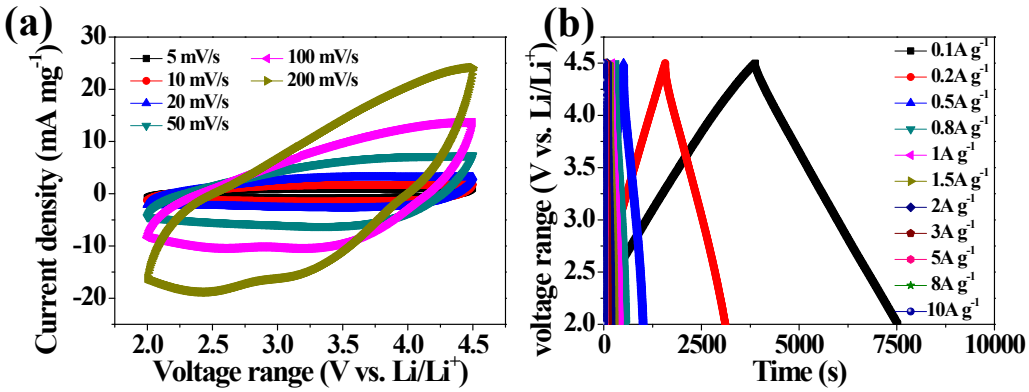

Figure S5. Electrochemical performance of a-EW sample. (a) CV curves and (b) GCD curves of a-EW.

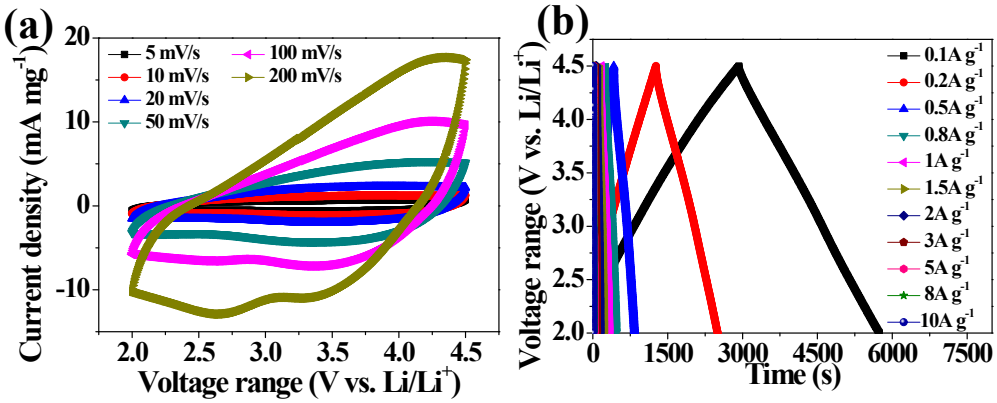

Figure S6. Electrochemical performance of commercial AC sample. (a) CV curves and (b) GCD curves of commercial AC.

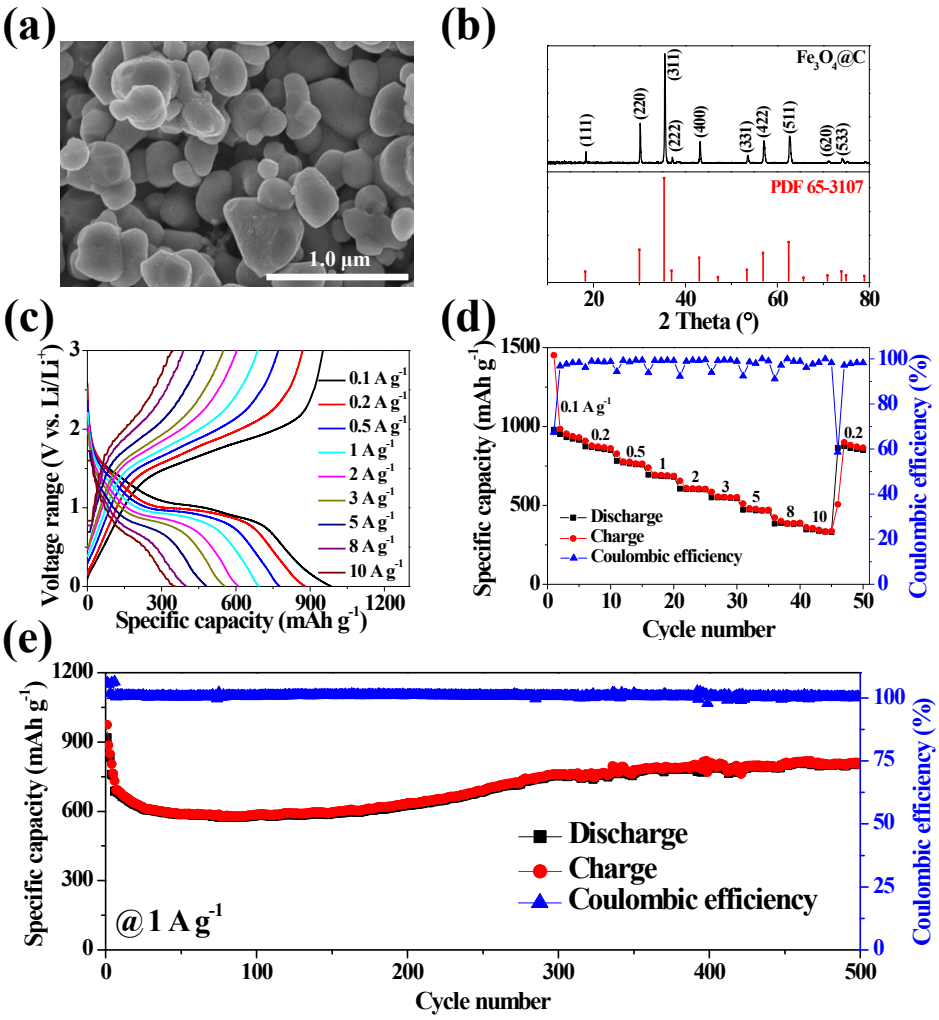

Figure S7. (a) SEM image and (b) XRD curves of Fe_3O_4@C nanoparticles. (c) charge/discharge curves of Fe_3O_4@C anode. (d) Specific capacity and (e) cycle performance of Fe_3O_4@C anode.

Before fabricating the LIC, the morphology and structural characterization, as well as electrochemical performance of Fe_3O_4@C anode were performed. As shown in **Figure S7a**, the morphology of Fe_3O_4@C are small independent particles with size in the range of 200~500 nm. XRD profile of Fe_3O_4@C shows well defined diffraction peaks, which agrees well with the standard XRD data of spinel magnetite (Fe_3O_4, JCPDS card 65-3107), suggesting the good crystallinity of Fe_3O_4@C (Figure S7b). The electrochemical performance of Fe_3O_4@C anode was also investigated in a Li half-cell system over a voltage range from 0.005 to 3.0 V vs. Li/Li^+. The GCD profiles of Fe_3O_4@C at different current densities (from 0.1 to 10 A g^{-1}) are shown in Figure S7c. All the GCD profiles demonstrate an obvious discharge plateaus, which is attribute to the

conversion of Fe_3O_4 to metalic Fe. The Fe_3O_4@C anode exhibit reversible capacities of 979.2, 873.2, 781.6, 694.1, 605.3, 550.3, 472.3, 384.5 and 347.3 mAh g^{-1} at current densities of 0.1, 0.2, 0.5, 1, 2, 3, 5, 8 and 10 A g^{-1}, respectively (Figure S7d). In addition, the Fe_3O_4@C anode displays a high capacity retention of 87.3% after 500 cycles at 1 A g^{-1}, demonstrating excellent electrochemical performance (Figure S7e). It is worth to notice that before fabricating the hybrid device, the Fe_3O_4@C anode was pre-activated for 5 cycles at 0.1 A g^{-1} in a Li half-cell and then discharged at 1.0 V vs. Li/Li^+ to achieve high efficiency.

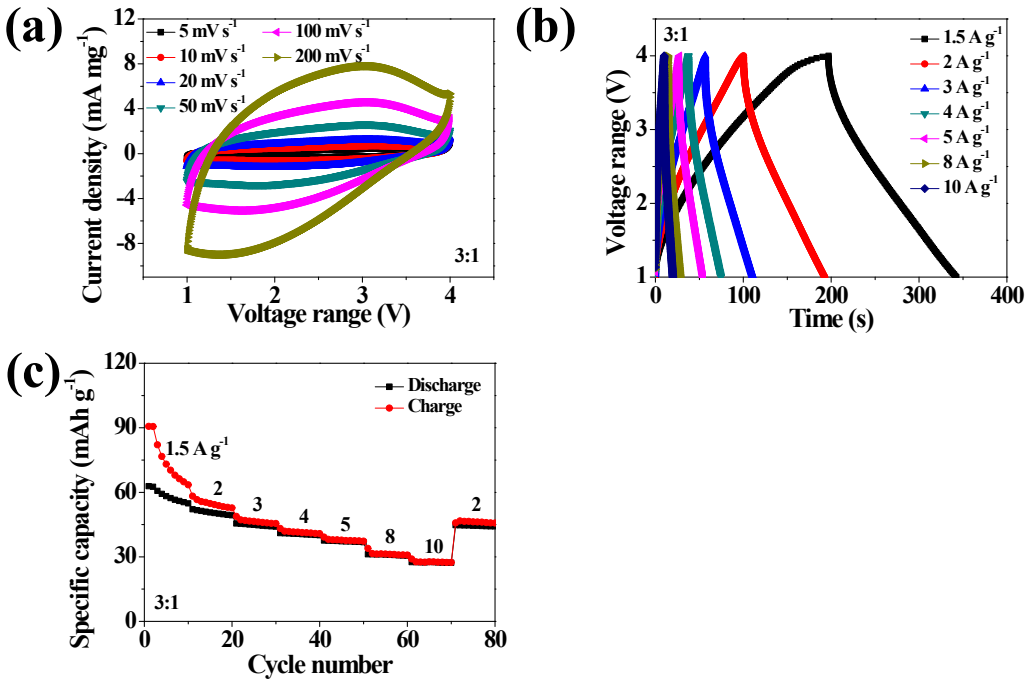

Figure S8. Electrochemical performance of a-EW-NaCl//Fe_3O_4@Cbased LIC device with a mass ratio of 3:1. (a) CV curves, (b) GCD curves and (c) specific capacities at different current densities of the a-EW-NaCl//Fe_3O_4@C based LIC with a mass ratio of 3:1.

Table S1. Cycling performance comparison with literature reported LICs.

Anode	Cathode	Voltage range	cycles	Capacity retention	Ref.
Fe_3O_4@C	a-EW-NaCl	1.0~4.0 V	2,000	88.3%	This work
LTO	AC	1.0~3.0 V	2,000	85.2%	S7
LTO	ZHTP	1.0~3.0 V	2,000	85%	S13
LTO	KC21-900	1.0~3.0 V	10,000	76%	S11
SnO_2-C	TMC	0.5~4.0 V	2,000	80%	S4
MnO/C	CNS	1.0~4.0 V	5,000	70%	S3
BNC	BNC	0~4.5 V	5,000	81%	S14

Footnote: M-LTO: AC: activated carbon; KC21-900: Prosopis juliflor treated at 900 °C; ZHTP: activated carbon derived from coconut shells; TMC: tubular mesoporous carbon; BNC: boron and nitrogen dual-doped 3D carbon nanofiber; CNS: carbon nanosheets;

Table S2. Energy and power density comparison with literature reported LICs.

Positive electrode	Negative electrode	Voltage window	Energy density (Wh kg^{-1})	Power density (W kg^{-1})	Ref.
EW-NaCl	Fe_3O_4@C	1.0-4.0 V	124.7	2547.4	This work
3D Graphene	Fe_3O_4/graphene	1.0-4.0 V	86	2587	S1
AC	hard carbon	1.5-3.9 V	60	~2250	S2
2D carbon nanosheet	2D MnO/C	1.0-4.0 V	100	83	S3
tubular mesoporous carbon	SnO_2-C	0.005-4.5V	110	~170	S4
AC	M-LTO	1.5-2.8 V	51.56	161.9	S5
SCDCS	SCDCS	0-4.5 V	124.8	107	S6
AC	LTO	1.0-3.0 V	79.6	~200	S7
SFAC-2	GC	2.0-4.0 V	104	143	S8
HDMPC	HDMPC	1.0-4.0 V	106.4	500	S9
AC	HC	1.5-4.2 V	100	150	S10
KC21-900	LTO	1.0-3.0 V	80	~200	S11

AC	MnNCN	0.1-4.0 V	103	~150	S12
ZHTP	LTO	1.0-3.0 V	69	~500	S13
BNC	BNC	0-4.0 V	104	22500	S14

Reference:

[S1]. F. Zhang, T. Zhang, X. Yang, L. Zhang, K. Leng, Y. Huang and Y. Chen, *Energy Environ. Sci.*, 2013, **6**, 1623-1632.

[S2]. A. Ohtomo and H. Y. Hwang, *Nature*, 2004, **427**, 423-426.

[S3]. Y. Zhao, Y. Cui, J. Shi, W. Liu, Z. Shi, S. Chen, X. Wang and H. Wang, *J. Mater. Chem. A*, 2017, **5**, 15243-15252.

[S4]. W.-H. Qu, F. Han, A.-H. Lu, C. Xing, M. Qiao and W.-C. Li, *J. Mater. Chem. A*, 2014, **2**, 6549-6557.

[S5]. D. Ruan, M.-S. Kim, B. Yang, J. Qin, K.-B. Kim, S.-H. Lee, Q. Liu, L. Tan and Z. Qiao, *J. Power Sources*, 2017, **366**, 200-206.

[S6]. X. Xu, Y. Cui, J. Shi, W. Liu, S. Chen, X. Wang and H. Wang, *RSC Adv.*, 2017, **7**, 17178-17183.

[S7]. B. Li, H. Zhang, D. Wang, H. Lv and C. Zhang, *RSC Adv.*, 2017, **7**, 37923-37928.

[S8]. Z. Yang, H. Guo, X. Li, Z. Wang, J. Wang, Y. Wang, Z. Yan and D. Zhang, *J. Mater. Chem. A*, 2017, **5**, 15302-15309.

[S9]. J. Niu, R. Shao, M. Liu, J. Liang, Z. Zhang, M. Dou, Y. Huang and F. Wang, *Energy Storage Mater.*, 2018, **12**, 145-152.

[S10]. J. Ajuria, E. Redondo, M. Arnaiz, R. Mysyk, T. Rojo and E. Goikolea, *J. Power Sources*, 2017, **359**, 17-26.

[S11]. P. Sennu, H.-J. Choi, S.-G. Baek, V. Aravindan and Y.-S. Lee, *Carbon*, 2016, **98**, 58-66.

[S12]. C. Liu, C. Zhang, H. Fu, X. Nan and G. Cao, *Adv. Energy Mater.*, 2017, **7**, 1601127.

[S13]. A. Jain, V. Aravindan, S. Jayaraman, P. S. Kumar, R. Balasubramanian, S. Ramakrishna, S. Madhavi and M. P. Srinivasan, *Sci. Rep.*, 2013, **3**, 3002.

[S14]. Q. Xia, H. Yang, M. Wang, M. Yang, Q. Guo, L. Wan, H. Xia and Y. Yu, *Adv. Energy Mater.*, 2017, **7**, 1701336.